Proceedings 10th NUMGE 2023
10th European Conference on Numerical Methods in Geotechnical Engineering
Zdravkovic L, Kontoe S, Taborda DMG, Tsiampousi A (eds)

https://doi.org/10.53243/NUMGE2023-26

The effect of finite layer thickness; a validation of MPM analysis by centrifuge testing

C. Zwanenburg[1,2], B. Wittekoek[1] , M. Martinelli[1,2], E.A. Alderlieste[3]

[1]*Deltares, Delft, the Netherlands*
[2] *Delft University of Technology, Delft, the Netherlands*
[3]*Equinor, Oslo, Norway*

ABSTRACT: A series of 4 plate loading tests on peat has been conducted in the centrifuge, to study the effect of finite layer thickness and to validate numerical techniques that capture large strain effects. The tests comprise a wide and small plate with smooth and rough boundary conditions. Remarkably, despite the applied displacement rate of 15 mm/min, the peat behaves partly or even nearly drained, providing a relatively large resistance. A clear difference in failure mechanism is found for the large and small plate. Numerical analysis is conducted using the material point method, MPM. The failure mechanisms and load displacement curves are well captured by the analysis when increasing the strength beyond the values found in conventional laboratory test data. Larger differences are found for analysis of the wide plate, which is explained by the irregularities induced by failure plane development and heterogeneity in the peat layer. For the small plate the finite layer effect influences the load when displacements reach 70% of the original layer thickness. Numerical analysis shows that the depth at which the finite layer effect influences the load -displacement curve is different for drained and undrained behaviour.

Keywords: large strain; centrifuge testing; MPM

1 INTRODUCTION

Construction activities in soft organic soils often induce large deformations, which might result in geometrical non-linearities, like finite layer thickness effects. Recent developments in geomechanics include the availability of numerical tools that do account for large strain effects. An example of such a method is the material point method, MPM, Fern et al. (2019).

For validation purposes a series of centrifuge tests has been conducted. The test series comprises large deformation plate loading tests with a plate displacement almost equal to the initial layer thickness. Speswhite clay and decomposed peat have been used as a foundation layer. This paper focusses on the tests on peat. The entire dataset for all tests is freely available, Zwanenburg et al. (2023)

2 TEST SET-UP

The model consisted of a 0.20 m thick peat layer which was placed in a strong box with inner dimensions of 0.20 m × 0.45 m × 0.87 m (W × H × L). During the tests, plates of 0.10 m and 0.02 m width were placed at the centre of the model, see Figure 1. To minimize the friction between the plate and front and back wall, the length of the plate perpendicular to the model was 0.195 m, thereby leaving some space between the plates and sidewalls. Consolidation was allowed at top and bottom of the peat layer. To prevent the peat layer from drying out, a water layer was placed on top. Tests were conducted for smooth, polished aluminium, and rough boundary conditions by sticking skateboard grip tape on the bottom plate and bottom of the loading plate. To allow drainage at the bottom, a grid of 76 holes, diameter 4.8 mm, was created. The holes were closed by a porous filter from sintered titanium with a pore size of 10 µm. The summed area of the porous filters was less than 1% of the area of the bottom plate and is therefore assumed not to influence the bottom friction. This resulted in; **test 1**: wide plate and smooth boundary conditions, **test 2**: wide plate and rough boundary conditions, **test 3**: small plate and smooth boundary conditions, **test 4**: small plate and rough boundary conditions.

Figure 2 shows an overview of the applied instrumentation. In total 16 total pressure cells were placed in the bottom and walls of the strong box. Nine pore pressure transducers were placed in the bottom plate and 2 were placed in the loading plate. Displacements were measured by 4 displacements transducers, DCDTs, not shown in Figure 2. Artificial texture was added on the side of the peat layer to improve PIV analysis.

Each test contained 3 phases. In the first phase, the centrifuge was accelerated to 100 g at 10 g/min. The

second phase consisted of consolidation, until the excess pore water pressure was less than 1 kN/m^2. It should be noted that due to the low density of peat, the generated excess pore water pressure was small. The third phase contained the actual test in which the plate was pushed into the soil with a constant displacement rate of 15 mm/min. To avoid overloading of the equipment, penetration was stopped 4 mm above the bottom of the peat layer or when the maximum measured pressure reached 1 MN/m^2.

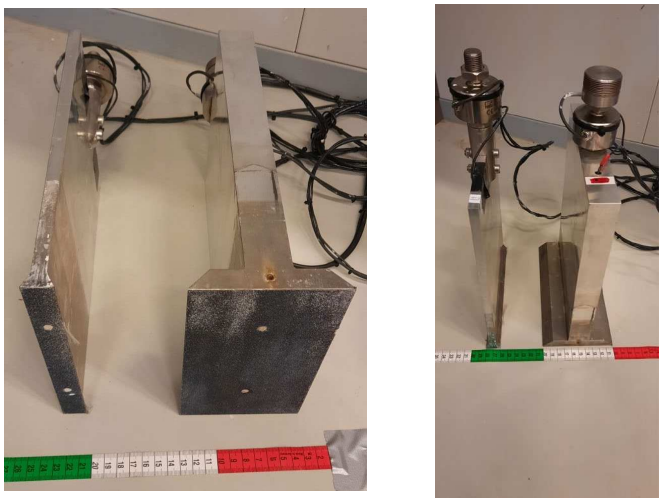

Figure 1. Loading plates with two pore pressure transducers at the bottom.

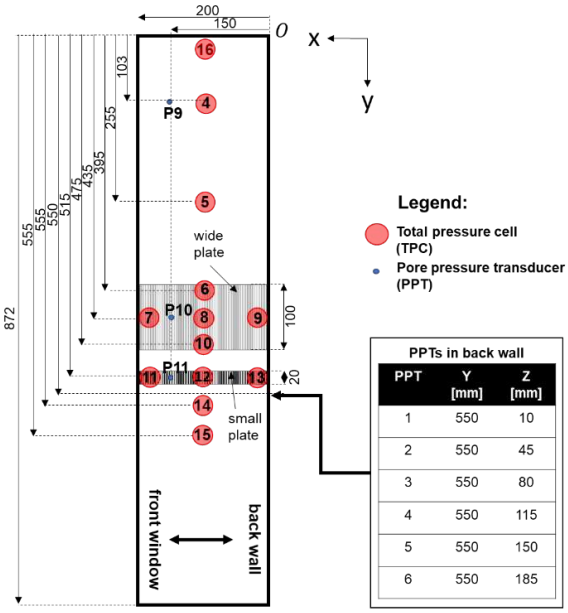

Figure 2. Instrumentation, dimensions in [mm], z = 0 at the bottom plate and upward pointing

3 TESTED MATERIAL

Humified peat was selected to be used as foundation layer. The organic nature of the material was expected to provide a soft, strongly deformable material. Due to the humification, no visible fibres are present. The low fibrosity of the material was believed to make the material suitable for centrifuge testing.

The material was sampled near Delft, the Netherlands, using the Deltares Large Diameter Sampler, DLDS (Zwanenburg, 2017), allowing for samples with a height of 1.0 m and diameter of 0.40 m. The peat layer had a thickness of approximately 0.9 m and was overlain by 2.3 m thick silty clay deposit.

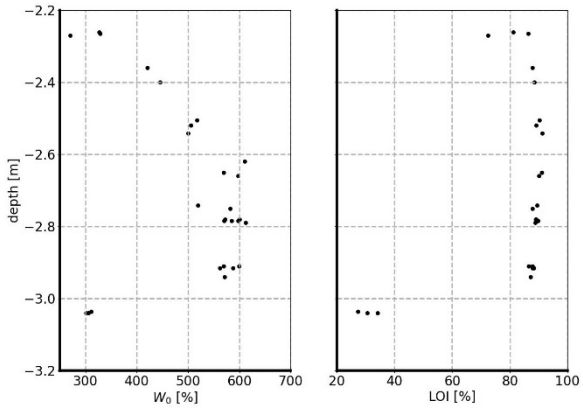

Figure 3. Characterisation of the tested material, a) initial water content, W_0, b) Loss on Ignition, LOI.

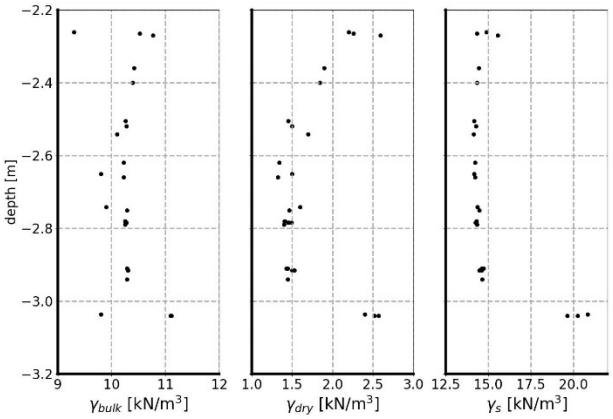

Figure 4. Characterisation of the tested material. a) bulk density, γ_{bulk}, b) dry density, γ_{dry}, b) solid density, γ_s.

An extended series of laboratory tests was conducted, including 5 constant rate of strain, CRS tests, 16 direct simple shear tests, DSS and 6 triaxial compression tests. Figures 3 and 4 plot the characterisation of specimens as function of depth. The values for W_0 and γ_{dry} seem to indicate more humification at the top 0.4 m.

Due to the required dimensions for the peat block to be tested, the blocks were cut in vertical direction from the sample and placed horizontally in the model. This introduced a 90° rotation. To understand the impact of this rotation, conventional laboratory tests were conducted on specimen obtained in horizontal and vertical directions.

Figure 5 shows a comparison of the over consolidation ratio, OCR, values in the peat layer. It should be noted that the OCR for the horizontally obtained samples is derived from the ratio $\frac{\sigma_{vy'}}{K_0^{OC}\sigma_{vi'}}$. Here, $K_0^{oc} = K_0^{NC} OCR^m$. In which σ'_{vy} represents the vertical yield

stress, σ'_{vi} the initial vertical effective stress, K_0^{oc} the lateral stress ratio for normally consolidated conditions. The power m is estimated based on the mean loss of ignition of 81.2% and approximately equal to 0.86. K_0^{NC} is estimated based on the internal friction angle derived from the DSS tests according to $1 - sin\varphi'$ with $\varphi' = 30°$. Although the number of observations is small, the OCR obtained from horizontally obtained samples seems larger than found for the vertically aligned samples. Also, the OCR decreases over depth. The permeability of the peat is in the order of 1.5×10^{-8} m/s.

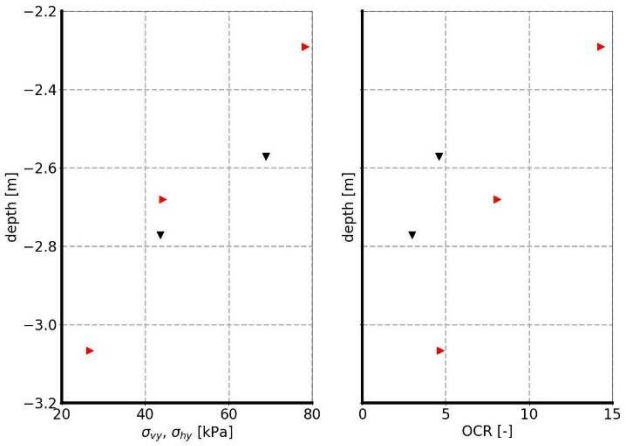

Figure 5. Comparison of yield stress and OCR values of specimens obtained in horizontal (red right pointing arrow) or vertical direction (black down pointing arrow).

To illustrate the anisotropy in strength behaviour, Figure 6 shows the results of undrained DSS tests on horizontally and vertically retrieved samples. The tests are conducted in accordance to ASTM D6528-07, in which undrained conditions are simulated by constant height, Dyvik et al. (1987). For Normally consolidated conditions, right graphs in Figure 6, no differences between the horizontally and vertically aligned specimens are found, and therefore, no strength anisotropy is assumed. In contrast, clear differences are found for the OC-conditions. At low stresses, large OCR, the horizontally aligned specimens reach lower strengths than found in the vertically aligned specimens, while for medium stress horizontally aligned specimens show dilative behaviour whereas vertically aligned specimens show contractive behaviour.

The undrained shear strength, s_u can be expressed as function of OCR (Ladd, 1991):

$$s_u = S\, OCR^m\, \sigma'_v \qquad (1)$$

In which S represents the undrained shear strength ratio, m a power and σ'_v the vertical effective stress. Table 1 shows the results of fitting eq. (1) to all the data. R^2 represents the weighted least squares sum, with $R^2 = 1.0$ for a perfect fit. The results are given for the peak strength, which is the largest strength measured during the test and the residual strength, which is the strength measured at maximum strain. The good match suggests that the anisotropy observed in strength follows from the anisotropy in OCR. This agrees with the observation that for the NC-tests no differences between the horizontal and vertical aligned specimens are found.

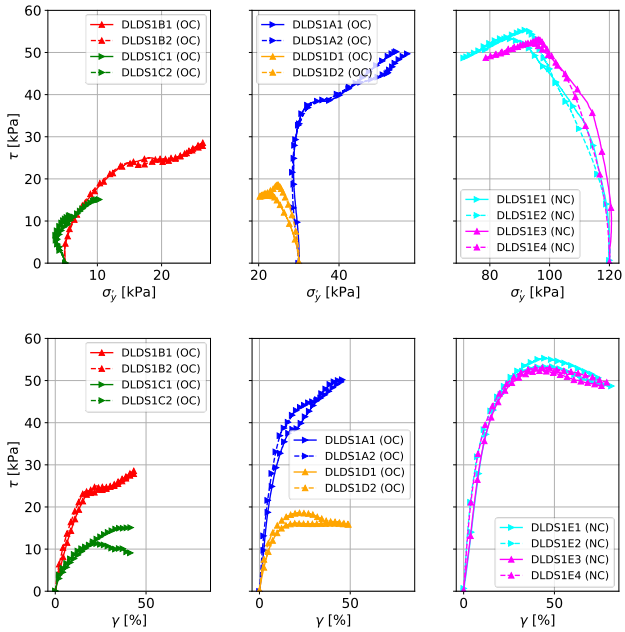

Figure 6. Stress paths (top) and stress – strain curves (bottom) of undrained DSS tests, right pointing arrows indicate horizontal aligned specimen, up pointing arrows indicate vertically aligned specimen.

Table 1. Results of curve fitting Equation (1) to the data

	peak	**residual**
shear strength ratio, S	0.42	0.42
power, m	0.86	0.87
R^2	0.90	0.93

4 TEST RESULTS

Distinct differences in failure mechanisms are found between the wide and small loading plate, see Figure 7. For the wide loading plate, a clear slip plane is found. Section 2 explained that the peat was rotated 90° to its original orientation. The slip planes in Figure 7a and b developed in the direction of the original top which seemed more humified as shown by Figure 3 and 4. The gap between the shaft and surrounding soil remains open at both sides. The small loading plate induces a punching shear failure and no clear slip planes are visible. The soil mass influenced by the plate displacements seems narrow and no gap is present between the shaft and surrounding soil. In all cases the shaft of the loading plate is initially aligned vertically.

The wide plates started tilting when approaching maximum displacement.

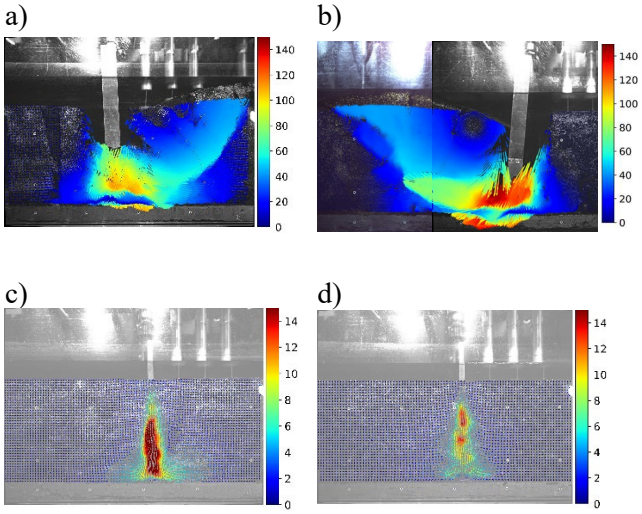

Figure 7. Displacement field at the end of the test, a) test 1, b) test 2, c) test 3, d) test 4, displacements in [mm].

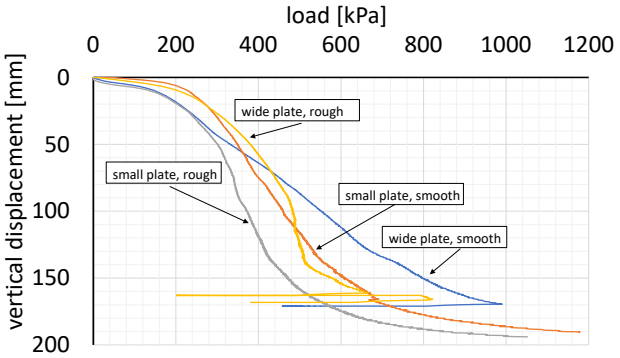

Figure 8. Load – displacement curves

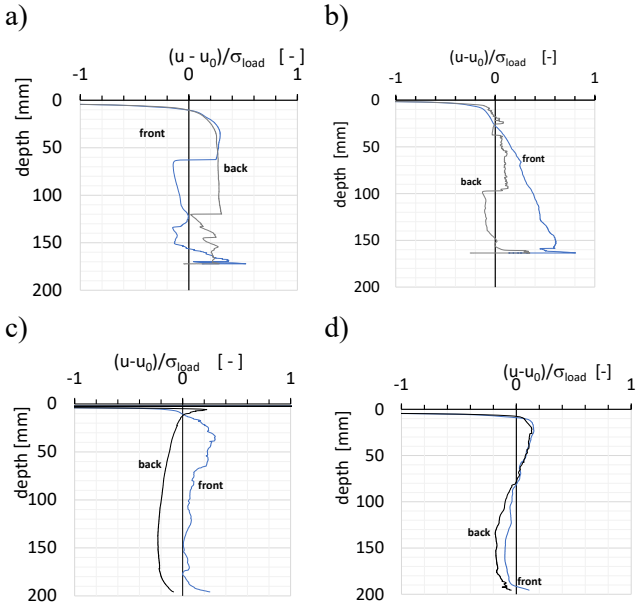

Figure 9. Pore pressure ratio at the front and back of the plate for a) test 1, b) test 2, c) test 3, d) test 4.; u = measured pore pressure, u_0 = hydrostatic pore pressure, σ_{load} = load exerted on the plate.

Figure 8 shows the load displacement curves found in the 4 tests. The small loading plates clearly show a strong increase in resistance when approaching the bottom of the peat layer. The tests with the wide plates were stopped earlier, when pore pressure transducers reach their maximum value and overloading of the transducers was avoided. It is remarkable that for rough boundary conditions a lower resistance is found than for the smooth boundary conditions. Uptil now, no satisfying explanation for this observation is found.

The level of drainage during plate displacement is found from the readings of the transducers mounted on the plate. Figure 9 shows the development of the dimensionless pore pressure ratio. The wide plate shows a larger pore pressure response than the small plate, which is easily explained by the dimensions of the plate. However, even for the wide plate the pore pressure is small and the tests can be considered partly or even fully drained. Figure 9a shows a rapid reduction in pore pressure at a depth of 80 and 120 mm and 9b at 100 mm. This is explained by the development of the sliding planes.

5 NUMERICAL ANALYSIS

5.1 Numerical model

Several recent studies support the suitability of MPM for the large-deformation analysis of penetration problems in soils, including pile installation (Kafaji, 2013) and CPT testing (a.o. Ceccato et al, 2016; Salgado et al. 2022; Martinelli and Pisano, 2022; Martinelli and Galavi, 2021, 2022). In this paper, the MPM formulation of Martinelli and Galavi (2022) is adopted to simulate the installation of the plate in peat. The salient features of the numerical model are:

- dynamic MPM formulation, with soil acceleration used primary unknown variable (Jassim et al., 2013);
- explicit, conditionally stable time integration, with automatic CFL-based adaptation of the time step size;
- simulation of plate–soil detachment and sliding using the contact algorithm by Bardenhagen et al. (2000);
- background mesh formed by four-node quadrilatedal elements;
- The concept of ‘moving mesh’ was used to ensure fine discretisation around the soil-plate interface and accurate performance of the contact algorithm (Kafaji, 2013).

Additional computational aspects regarding e.g. mass scaling and numerical damping are covered in Martinelli & Galavi (2022). The computational mesh

is shown in Figure 10, for both wide and small plate. The contact between the plate and the soil is perfectly smooth. At all boundaries, the displacements are constrained in perpendicular direction and free in the longitudinal one. A set of fixed material points is used to apply a fixed boundary condition to the domain. The mesh moves together with the plate, whereas this set of material points remains fixed in space in order to simulate the effect of the rigid container.

The Soft Soil model (Bentley, 2022) is used as constitutive model, see Table 2 are for applied parameters. Figure 6 shows that the simulations are in satisfactory agreement with the experimental data.

The MPM model is used to simulate both drained and undrained tests. In the latter ones, the bulk modulus of water is set to 20 MPa, which is lower than the true value of 2 GPa to decrease the computational time, while still being large enough to get a high equivalent undrained Poisson's ratio ν_u.

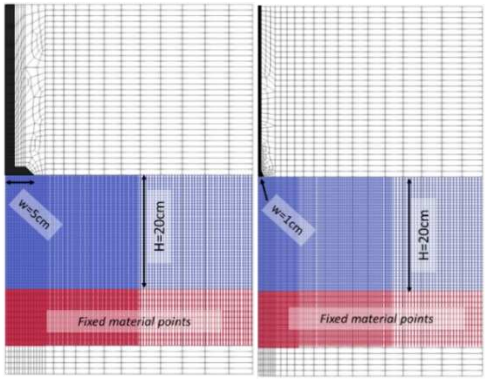

Figure 10: Computational mesh for the wide (B=100mm) and small (B=20 mm) plates.

Table 2: reference input parameter for the Soft Soil model.

Parameter	*value*	*description*
γ_{sat} [kN/m^3]	10.3	Bulk unit weight
n [-]	0.88	Porosity
OCR [-]	5	Over consolidation ratio
λ^* [-]	0.206	Modified compression index
κ^* [-]	0.0262	Modified swelling index
c [-]	10.0	Effective cohesion
φ' [°]	40.0	Friction angle
ψ [°]	0.0	Dilation angle
σ_t [kPa]	6.2	Tensile strenght
ν [-]	0.3	Poisson's ratio for unl./reload
K_0^{NC} [-]	0.33	Coefficient of lateral stress

5.2 Results

The simulations are performed using the reference parameters, labeled as A_{ref}. Simulation *B01* indicates the use of values for cohesion and friction angle set to 20 kPa and 35° , respectively; whereas the simulation *B02* refers to the 40 kPa and 30 °.

The load-displacement curves are shown in Figure 11. In all cases, the load monotonically increases with the penetration depth, and the values abruptly increase when the plate approaches the bottom of the container, in agreement with the experimental data.

For the small plate, the drained numerical results agree well to the experimental data, and the assumption of drained condition is also consistent with the experimental observations in Figure 9. The reference parameters (A_{ref}) provides a lower initial stiffness compared to the experimental data, and a better fit is obtained with a higher cohesion. The undrained simulations give a much lower bearing capacity and a much softer load-displacement curve.

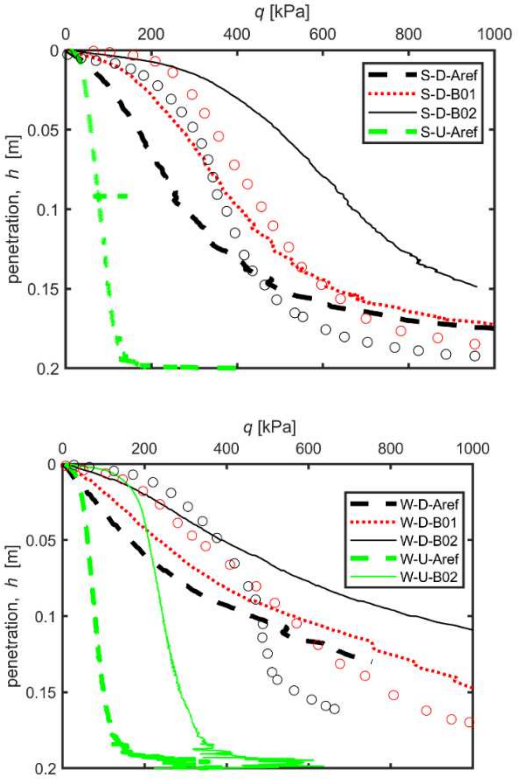

Figure 11: Drained (W-D) and undrained (W-U) simulations. MPM results against experimental data. Top: Small plate (B=20 mm), below: Wide plate (B=100 mm), open circles represent measurement data

For the wide plate, the drained numerical results, despite an initial low stiffness, tend to overpredict the bearing capacity. As for B=20mm, a higher value of cohesion provides a better fit for the initial stiffness but it significantly overestimates the foundation load at large penetration depth. For the wide plate, the non-negligible excess pore pressures measured during the test, Figure 9, may support the hypothesis of a partially-drained hydraulic conditions instead of fully-drained. The development of excess pore pressures results in a load-displacement curve which is between the drained and undrained ones, and then close to the experimental data. This hypothesis will be verified in a follow-up study, where 2-phase coupled simulations will be performed.

Figure 12 shows the distribution of the deviatoric strains computed in drained simulations for B=20mm and 100 mm, respectively. Figure 12 shows similar failure pattern compared to the experimental data.

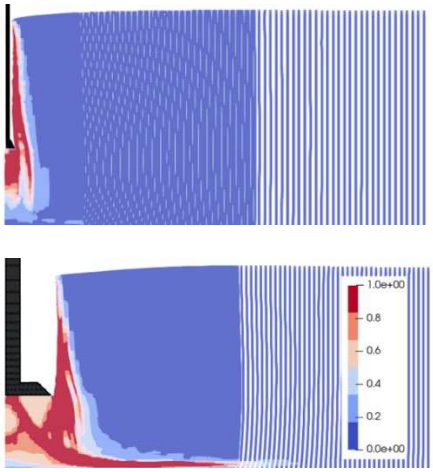

Figure 12: Drained simulation. Distribution of deviatoric strains after 130 mm of penetration. Top: Small plate (B=20 mm), below: Wide plate (B=100 mm).

6 DISCUSSION & CONCLUSIONS

A series of 4 plate loading tests has been conducted on peat in a centrifuge. The roughness of the bottom and plate does not seem to influence the results. A remarkable difference is found between the tests with a wide plate, which induce a clear failure mechanism and small plates which induce punching shear. Despite the applied displacement rate of 15 mm/ min, the peat behaves largely drained. When reaching maximum displacement the load clearly increases. Numerical analysis shows a good reproduction of the observed failure mechanisms, but needs some adjustment of the strength parameters to capture the load - displacement curve.

The tests show a clear influence of the effect of the finite layer thickness in a load increase. The numerical simulations capture this effect well. Remarkably, the analysis shows that for undrained conditions, the finite layer effect is only relevant close to the final depth, during the last 10 mm displacement before hitting the bottom.

For the wide plate, numerical analysis does not correspond well to the experimental data. This is explained by the development of discrete failure planes and the fact that these failure planes are influenced by heterogeinity in the peat layer, which is not accounted for in the numerical analysis. Despite the development of the sliding planes, the measurements for the wide plate also show the influence of the finite layer thickness. Numerical analysis shows that also for the wide plate the finite layer effect is stronger for drained conditions than found in undrained conditions.

7 ACKNOWLEDGEMENTS

We would like to acknowledge Deltares for funding this study and the technician team to conduct the experiments. Furthermore, we thank Hans Teunissen for his support and assistance in exploring the phenomenon of geometrical non-linearities. The MPM simulations are performed using a version of Anura3D developed in-house by Deltares. Works not executed for Equinor.

8 REFERENCES

Bardenhagen, S., Brackbill, J. & Sulsky, D. 2000. The material point method for granular materials. *Comput. Methods Appl. Mech. Eng* 187, No. 3–4, pp. 529–541.

Bentley 2022. PLAXIS, Material Models Manual.

Ceccato F., Beuth L., Vermeer P.A., Simonini P. 2016. Two-phase material point method applied to the study of cone penetration *Computers and Geotechnics* 80 (2016)440-452 doi: 10.1016/j.compgeo.2016.03.003

Dyvik, R., Berre, T., Lacasse, S., & Raadim, B. 1987. Comparison of truly undrained and constant volume direct simple shear tests, *Géotechnique* **37,** No.1, 3-10.

Fern, J., Rohe, A., Soga, K., Alonso, E. 2019. The Material Point Method for Geotechnical Engineering, A Practical Guide, CRC Press, Taylor & Francis Group, New York.

Jassim, I., Stolle, D. & Vermeer, P. 2013. Two-phase dynamic analysis by material point method. *Int. J. Numer. Anal. Methods Geomech*. 37, No. 15, pp. 2502–2522.

Kafaji, I. K. 2013. Formulation of a dynamic material point method (MPM) for geomechanical problems. Ph.D. thesis, University of Stuttgart.

Ladd, C.C. 1991. Stability Evaluation During Staged Construction, the 22nd Karl Terzaghi lecture, *Journal of Geotechnical Engineering,* Vol. 117(4), pp. 540-615.

Martinelli, M. & Galavi, V. 2021. Investigation of the material point method in the simulation of cone penetration tests in dry sand. *Comput. Geotech*. 130, 103923.

Martinelli, M. & Galavi, V. 2022. An explicit coupled MPM formulation to simulate penetration problems in soils using quadrilateral elements, *Computers and Geotechnics* 145 (2022), 104697.

Martinelli, M., & Pisanò, F. 2022. Relating cone penetration resistance to sand state using the material point method. Géotechnique Letters 12, 1–8,10.1680/jgele.21.00145

Salgado R., Bisht V., Prezzi M. 2022. Material Point Method simulations of cone penetration and CPT interpretation *in: Cone Penetration Testing 2022 (Gottardi & Tonni eds)* doi: 10.1201/9781003308829-2

Zwanenburg C. 2017. The development of a Large Diameter Sampler *Proceedings of the 19th International Conference on Soil Mechanics and Geotechnical Engineering, Seoul.*

Zwanenburg C. Wittekoek B., Martinelli M., Alderlieste E., Zwaan R. 2023. Calibration chamber for numerical tools, Zenodo, Accessed June 29, 2023 https://doi.org/10.5281/zenodo.8066899